CrystEngComm

Accepted Manuscript

ROYAL SOCIETY OF CHEMISTRY

www.rsc.org/crystengcomm

Cite this: DOI: 10.1039/c0xx00000x

www.rsc.org/xxxxxx

ARTICLE TYPE

Preparation, Magnetic and Microwave Absorption Properties of $MnNb_2O_6$ Ellipsoid-Like Hierarchical Structures

Shuijin Lei,*[a] Donghai Guo,[a] Chuanning Wang,[a] Di Cheng,[a] Xijie Gao,[a] Suyuan Zeng,[b] Yanhe Xiao[a] and Baochang Cheng[a]

Received (in XXX, XXX) Xth XXXXXXXXX 20XX, Accepted Xth XXXXXXXXX 20XX
DOI: 10.1039/b000000x

Great efforts have been made to synthesize columbite niobates due to their fascinating properties and applications. In this research, the ellipsoidal $MnNb_2O_6$ crystals have been successfully prepared by a facile hydrothermal method. X-ray powder diffraction patterns showed that the products have the typical orthorhombic columbite structure. The electron microscopy analysis revealed that the obtained $MnNb_2O_6$ ellipsoids had a very rough surface with flaky hierarchical structures composed of nanoparticles with the diameters of 10–20 nm. Based on the time-dependent experiments, a possible growth mechanism of the ellipsoidal hierarchitectures was also proposed. The magnetization studies demonstrate that the products exhibit an antiferromagnetic behavior with the Néel temperature of about 4 K. The microwave absorption properties of the ellipsoidal $MnNb_2O_6$ hierarchical structures were also investigated with a vector network analyzer. The absorbing peak position moves to lower frequency with increasing the thickness of sample. The value of the minimum reflection loss is −11.6 dB at 7.8 GHz with a matching thickness of 3.5 mm, and the reflection loss lower than −10 dB can be obtained in the frequency range of 7.2–8.3 GHz.

Introduction

The binary niobate ceramics, with a general formula ANb_2O_6 where A is a divalent alkaline-earth or transition metal cation with ionic radius less than 1 Å, usually crystallizes in the columbite structure. This class of materials have attracted much attention due to their interesting optical, dielectric, magnetic and catalytic properties, as well as the possible applications as a dielectric resonator and filter for use in the field of mobile and satellite communication.[1-2] Besides that, these dielectric ceramics have lower sintering temperatures than the perovskites.[3-7] To improve the quality factor, these compounds are always used as the precursor for the synthesis of some complex perovskites.[6-9]

As a typical member of the columbite niobate family, manganocolumbite ($MnNb_2O_6$) belongs to the very important multifunctional materials. Generally, $MnNb_2O_6$ exhibits antiferromagnetic ordering with the Néel temperature of about 4.4 K.[10-11] It is interesting that the introduction of Fe ions to form $Fe_xMn_{1-x}Nb_2O_6$ solid solution will destroy the antiferromagnetic order only found for the two end-members.[12] Besides dielectric behavior,[3-7] the electrical conductivity of $MnNb_2O_6$ is also a concern. It exhibits high dielectric losses at microwave frequencies due to some conductivity from variations of composition in nonstoichiometric system.[1,3,6] Experiments showed that the reduced (anion vacancy type) $MnNb_2O_{6-x}$ has an enormous increase in electrical conductivity.[13-15] What's more, the electrochemical insertion properties of $MnNb_2O_6$ as cathodes in lithium batteries were also studied.[16] Recently, Mansurova et al. have investigated the thermochemical properties of $MnNb_2O_6$.[17]

As we know, these prominent physical and chemical properties should be associated with its crystal structure. It is well-known that columbite can be considered as a superstructure of R-PbO_2.Then accordingly, in columbite $MnNb_2O_6$ structure with an orthorhombic symmetry, Mn and Nb atoms are surrounded by six oxygen atoms to form MnO_6 and NbO_6 octahedra, which share edges and form independent zigzag chains along the *c*-axis. Meanwhile, these parallel MnO_6 and NbO_6 layers alternate along the *a*-axis in the sequence Mn-Nb-Nb-Mn-Nb-Nb-Mn.[18]

There are various methods for the preparation of $MnNb_2O_6$. Among them, the solid state combination has always been the most popular technique for the synthesis of polycrystalline $MnNb_2O_6$ powders using stoichiometric mixtures of Nb_2O_5 and MnO or $MnCO_3$ at high temperatures (≥ 1100 °C).[3-7,12-14,16-17] However, multiple heating and regrinding steps are generally essential to overcome the solid state diffusion barrier. Additionally, the products always have irregular morphology and large particle size. To reduce the sintering temperature, the mechanochemical synthesis has been researched.[19] Bartels et al. prepared $MnNb_2O_6$ crystals using stoichiometric oxide mixture plus HF solution in a noble metal capsule by the high-temperature hydrothermal method at 800 °C.[20] $MnNb_2O_6$ nanoparticles were also prepared by Zhang et al. based on the nonaqueous sol–gel synthesis of niobium chloride and manganese acetylacetonate in benzyl alcohol at 200 °C.[21] Moreover, Hu et al. successfully fabricated $MnNb_2O_6$ flower-like structures by the solvothermal reaction of $NbCl_5$ and $MnCl_2$ employing cyclohexanol as the solvent.[22-23] As for the single-crystalline $MnNb_2O_6$, the common growth methods include flux growth,[24] Czochralski technique,[10-

[11,25] and floating zone method.[2]

Inspired by the promising physicochemical properties and extensive potential applications of $MnNb_2O_6$ materials, it is interesting and challenging to explore a simple synthetic approach to fabricate them with special morphology. In this research, a convenient and green hydrothermal process has been successfully used for the preparation of $MnNb_2O_6$ ellipsoid-like hierarchical structures and the magnetic and microwave absorption properties of the product have also been investigated.

Experimental

Chemicals and materials

All the chemicals and reagents were used as received without any further purification. Niobium pentoxide (Nb_2O_5), potassium hydroxide (KOH), tetrahydrated manganese chloride ($MnCl_2·4H_2O$) are of analytical grade purchased from Sinopharm Chemical Reagent Co., Ltd. (Shanghai, China).

Synthesis of $MnNb_2O_6$ ellipsoids

All samples were prepared by a hydrothermal method without any calcination treatment and the synthetic procedure can be described as follows. For the first step, the potassium polyoxoniobate ($K_7HNb_6O_{19}·13H_2O$) was obtained from the reaction of Nb_2O_5 powder with molten KOH followed with the recrystallization in aqueous solution according to the previous literature.[26] Regarding the typical synthesis of $MnNb_2O_6$ ellipsoids, 0.119 g of $MnCl_2·4H_2O$ (0.6 mmol) and 0.274 g of $K_7HNb_6O_{19}·13H_2O$ precursor (0.2 mmol) were respectively dissolved in 10 mL of distilled water. Subsequently, $MnCl_2$ solution was added dropwise into the polyoxoniobate solution under continuous magnetic stirring and the pale pink suspension could be formed. The resulting suspension was then transferred into a stainless steel Teflon-lined autoclave of 50 ml capacity, which was then filled with distilled water up to 80% of the total volume and stirred to be homogeneous. The autoclave was sealed and maintained at 150 °C for 24 h, and then cooled to room temperature naturally. The precipitates were filtered off and washed with absolute ethanol and distilled water several times to remove the soluble impurities, and then dried at 60 °C for 6 h in air. The earth-yellow powder could be obtained.

Sample characterization

The X-ray powder diffraction (XRD) patterns were recorded on a D8 Focus diffractometer with Cu-Kα radiation (λ = 1.5406 Å) (Bruker, Germany). The transmission electron microscopy (TEM), high resolution transmission electron microscopy (HRTEM) images and selected area electron diffraction (SAED) patterns were taken from a JEM-2010 transmission electron microscope (JEOL, Japan) with an accelerating voltage of 200 kV. For both TEM and HRTEM tests, after ultrasonic agitation, one or more drops of the ethanol solution containing the as-synthesized compound were deposited onto the amorphous carbon film supported on a copper grid and allowed to dry at room temperature in air. The scanning electron microscopy (SEM) measurements were preformed on a JSM-6701F (JEOL, Japan) field-emission scanning electron microscope. The magnetic properties data were collected on a Magnetic Property Measurement System (MPMS), SQUID−VSM (superconducting quantum interference device−vibrating sample magnetometer) (Quantum Design, USA). The as-prepared powdered sample was put into a gelatin capsule. The temperature dependence of the magnetization was measured under both zero-field-cooled (ZFC) and field-cooled (FC) modes in the temperature range of 1.8–300 K with an applied magnetic field of 0.01 T. For the detailed procedures, in the ZFC measurements, as the sample was cooled to 1.8 K in a zero magnetic field, an applied field was then introduced and the magnetization was recorded in a warming cycle. Then the FC measurements were conducted in a cooling cycle with an applied magnetic field. The isothermal magnetization measurements were carried out in a magnetic field that varied between +6 T and −6 T at different temperatures (1.8, 4, 8, 20, and 100 K). Before each run, for the sake of demagnetization, the sample was heated to room temperature and then cooled to the test temperature in a zero field. The complex dielectric permittivity ($\mu_r = \mu' - j\mu''$) and magnetic permeability ($\varepsilon_r = \varepsilon' - j\varepsilon''$) were obtained by a vector network analyzer (VNA, AV3629D) using transmission/reflection mode in the frequency range of 2–18 GHz. The as-prepared $MnNb_2O_6$ powder was mixed uniformly with molten paraffin wax and molded into toroidal-shaped specimen for microwave tests.

Results and discussion

Phase analysis

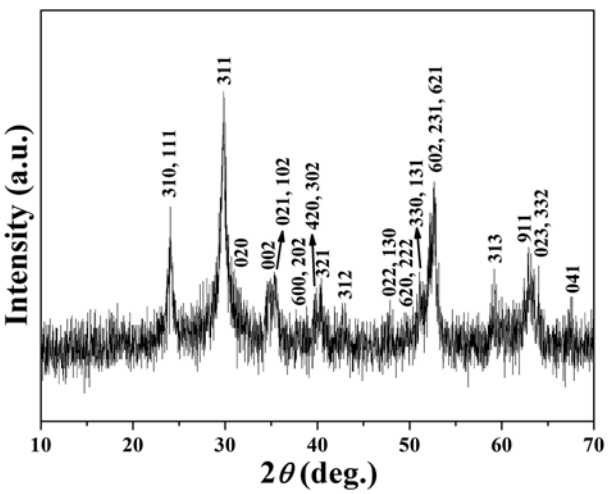

Fig. 1 XRD patterns of the sample synthesized at 150 °C for 24 h by hydrothermal treatment.

The phase purity of the as-prepared sample is studied by the XRD patterns as shown in Fig. 1. All the diffraction peaks can be indexed to the orthorhombic structure of $MnNb_2O_6$ with lattice constants of a = 14.428 Å, b = 5.751 Å and c = 5.095 Å, which are consistent with the reported values (JCPDS, Powder Diffraction File No. 72-0484, a = 14.420 Å, b = 5.760 Å and c = 5.083 Å). No characteristic reflection peaks derived from other contaminants such as manganese or niobium oxides, and other phases of manganese niobates can be detected, which indicates that the level of impurities in the sample is lower than the resolution limit of the XRD instrument.

Morphology analysis

The morphology of the products was examined by electron

microscopy images. Fig. 2a and 2b respectively presents the SEM and TEM image of the hydrothermal product at 150 °C for 24 h. From the SEM image, it can be seen that the sample consists of large-scale ellipsoidal crystals with diameters of about 100–200 nm. However, it is interesting that these ellipsoids have a very rough surface, on which some flake-shaped substructures can be observed (e.g. those ellipsoids marked in the rectangular marquee). These nanoflakes can be considered to cross each other along the long axis of the ellipsoids to form a carambola-like (star fruit-like) morphology. Furthermore, according to the TEM image displayed in Fig. 2b, it can be noted that these ellipsoidal hierarchical structures have an obvious polycrystalline nature and consist of nanoparticles with the diameters of about 10–20 nm. To further explore the microstructure of the as-obtained polycrystalline ellipsoids, the HRTEM and SAED analyses were undertaken from a single constituent nanoparticle. As shown in Fig. 2c, the HRTEM image shows clearly resolved two-dimensional atomic lattice fringes, suggesting a good crystallinity of these nanoparticles. Both interplanar spacings are identical and can be measured to be 0.3 nm with a separation angel of 76.8°, which match well with the (311) and ($\bar{3}$ 11) planes of orthorhombic columbite structure of $MnNb_2O_6$ phase. Fig. 2d presents the corresponding SAED patterns recorded along [0 $\bar{1}$ 1] zone axis, which also confirms the good single-crystalline structure. These results further demonstrate that the as-prepared product consists of $MnNb_2O_6$ pure phase.

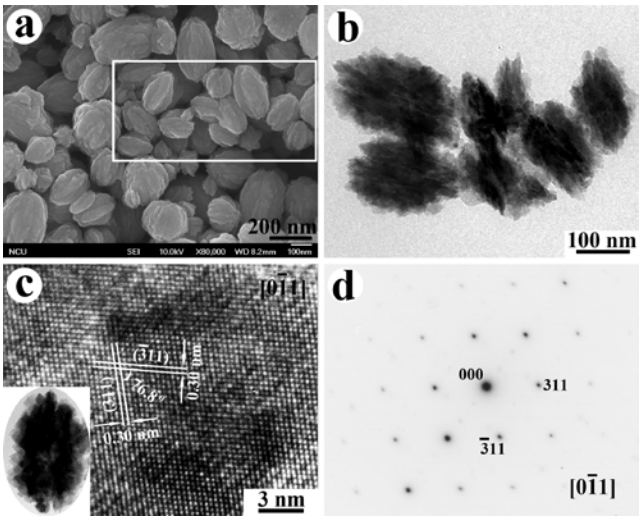

Fig. 2 (a) SEM, (b) TEM, (c) HRTEM images and (d) SAED patterns of the $MnNb_2O_6$ sample prepared via the hydrothermal route at 150 °C for 24 h.

Growth mechanism

In order to reveal the formation mechanism of the ellipsoidal $MnNb_2O_6$ hierarchical nanostructures, time-dependent reactions have been carried out to investigate the growth process in detail. Fig. 3 displays the SEM images of the products obtained from 3 to 12 h. In practice, experiments showed that if the reaction time was less than 3 h, the product still had a pink appearance and remained in an amorphous state (the corresponding XRD data not shown), so the $MnNb_2O_6$ crystalline phase could not be formed. Fig. 3a is the SEM image of the room temperature precursor prepared by the mixing of $MnCl_2$ and $K_7HNb_6O_{19}$ aqueous solutions, which is composed of a large quantity of nanoparticles with an average diameter of about 25 nm. After the hydrothermal treatment for 3 h, as shown in Fig. 3b, it can be found that these nanoparticles are inclined to aggregate. With the reaction time increasing, as expected, the larger spherical particles are formed (Fig. 3c). As prolonging the reaction time to 12 h, the particle size becomes further bigger. More importantly, those initial constituent nanoparticles turn into flake structures, which are arranged along a given direction to form the elongated spheres (Fig. 3d). When the reaction time was further increased to 24 h, these elongated spheres eventually evolve to the ellipsoids with flaky hierarchical structures as shown in Fig. 2. Considering the ripening and growth of these crystals, Fig. 3e shows the plot of mean particle size vs reaction time. First, before 3 h, there is only a very small increase in particle size, because crystallization is the main process in this period; Second, the particle size rapidly increases between 3~12 h, which implies the crystal growth process; Finally, after 12 h, the pace of size increase is obviously eased, since the crystals are almost formed.

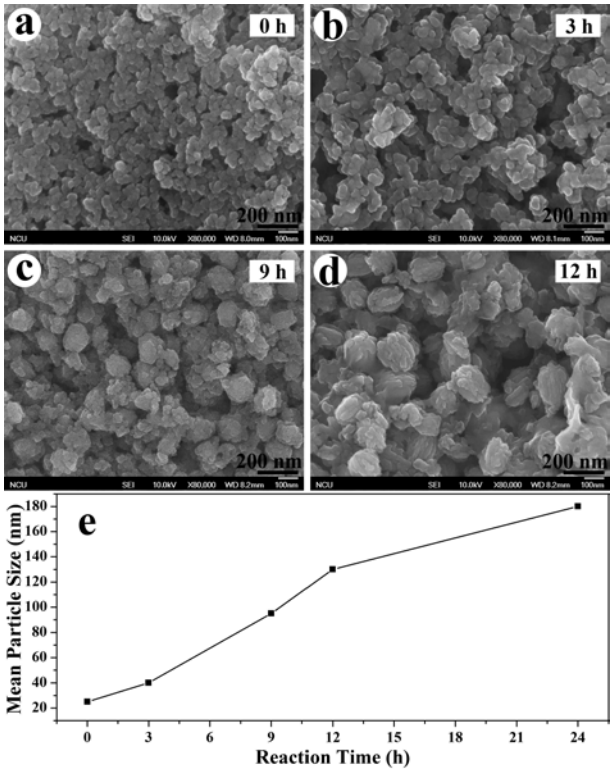

Fig. 3 SEM images of (a) the room-temperature product and the morphological evolution of the $MnNb_2O_6$ ellipsoid-like hierarchical structures prepared at different reaction time: (b) 3 h, (c) 9 h, (d) 12 h. (e) Variation of the mean particle size with the reaction time.

Based on the experimental results above, a possible growth mechanism of the ellipsoidal $MnNb_2O_6$ hierarchical nanostructures is proposed as illustrated in scheme 1. The obtained $MnNb_2O_6$ ellipsoids may be formed through the following processes. Initially, with the mixing of Mn^{2+} cations and $Nb_6O_{19}^{8-}$ anions, an immediate nucleation reaction occurs to form the primary amorphous nanoparticles. However, driven by minimizing the surface energy of the system, those nanoparticles tend to aggregate. When increasing the reaction temperature and prolonging the reaction time, the obtained nanoparticles keep

crystallizing at the expense of the amorphous contents. As a result, a concentration gradient will be formed between the inside and outside of the particles. The reaction ions in the solution are continually adsorbed on the surface of the particles to support the further growth. Owing to the assembly and coalescence together with the crystallization and growth of these nanoparticles, the larger-sized spherical particles are formed. Then, with further prolonging the growth time, the spheres will experience a secondary growth. As a result, the nanoflakes gradually appear on the spheres arising from Ostwald ripening of nanoparticles, and the spheres are elongated with a larger size. Finally, the further growth of the substructured nanoparticles and nanoflakes give rise to the formation of the ellipsoidal $MnNb_2O_6$ hierarchical structures. Although there is hardly any report on the isoelectric point of $MnNb_2O_6$, Kim et al. have demonstrated that the isoelectric point of $MgNb_2O_6$ and $PbNb_2O_6$ is about 3.0 and 3.9, respectively. Taking these as reference, it would be speculated that $MnNb_2O_6$ should have a similarly small isoelectric point. As the Mn^{2+} and $Nb_6O_{19}^{8-}$ precursor solutions are mixed, a rapid neutralization reaction should be certainly conducted. After then, experiments showed that the pH value of the system was near to neutral, indicating a large negative value of the Zeta potential. At this point, the K^+ cations may be expected to be adsorbed onto the surface of the particles, which is probably associated with the orientated growth of those nanoflakes to form the hierarchically ellipsoidal structure.

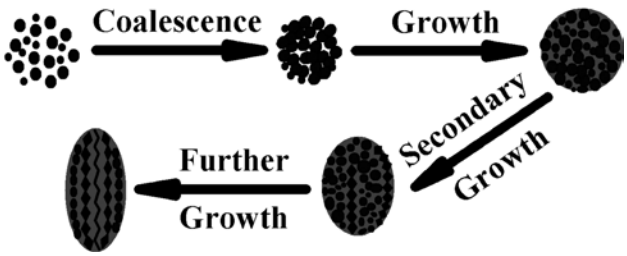

Scheme 1 Schematic illustration of the morphological evolution for the $MnNb_2O_6$ ellipsoid-like hierarchical structures at various stages.

Magnetic properties

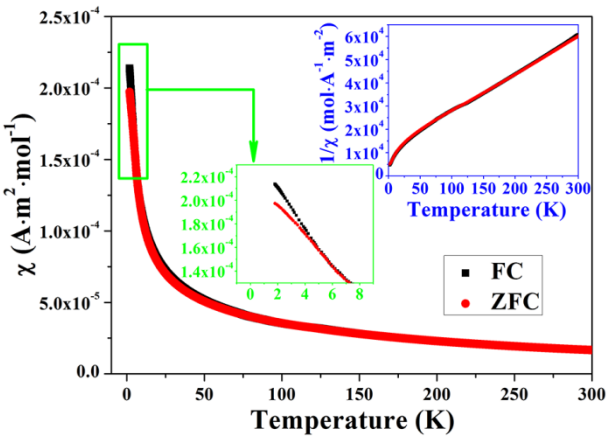

Fig. 4 The temperature dependence of the molar susceptibility curves (χ–T) of the as-prepared $MnNb_2O_6$ ellipsoidal sample in ZFC and FC processes measured at an applied magnetic field of 0.01 T. The left inset shows the close-up view of the antiferromagnetic transition temperature $T_N \approx 4$ K. The right inset presents the corresponding temperature dependence of the reciprocal molar magnetic susceptibility curves (χ^{-1}–T).

As shown in Fig. 4, the temperature dependence of the molar susceptibility (χ) for the as-prepared $MnNb_2O_6$ ellipsoids was measured during ZFC and FC processes from 1.8 to 300 K with an applied magnetic field of 0.01 T. It can be seen that the ZFC and FC curves are nearly superimposable at all test temperatures. In the temperature region above ~20 K, a small magnetization associated with the existence of paramagnetic and spin-disorder state can be observed. With decreasing the temperature, however, the ZFC and FC curves maintain overlapped and rise sharply. Actually, the two curves are not overlapped at very low temperatures. For easy identification, the ZFC and FC curves at a temperature region lower than 8 K are enlarged for a close-up view and shown in the left inset panel. A clear bifurcation between the ZFC and FC curves can be detected, suggesting a characteristic irreversibility. Previously, it has been well-reported that columbite $MnNb_2O_6$ exhibits antiferromagnetism at a very low temperature (4.4 K for single crystal).[10-11,18] Therefore, the separation between ZFC and FC magnetization curves indicates the transition from paramagnetic to antiferromagnetic order with the Néel temperature of $T_N \approx 4$ K, which is in good consistence with that reported in literatures. [10-11,18]

The right inset panel of Fig. 4 shows the reciprocal of the molar magnetic susceptibility as a function of temperature for the as-synthesized $MnNb_2O_6$ ellipsoidal sample. As expected, an obvious linear section at a very broad temperature region can be found in the χ^{-1}–T curve, which indicates that the product follows Curie–Weiss law in the paramagnetic state above T_N. The data can be then linearly fitted by a least-squares method to the equation $\chi = C/(T - \Theta)$, where C is the Curie constant related to the effective magnetic moment (μ_{eff}), T is the absolute temperature and Θ is the Weiss temperature. The Curie constant can be calculated from the slope of the fitted line to be $C = 5.95$, while the Weiss temperature should be obtained by extrapolating the fitted line to $\chi^{-1} = 0$ and intercepting the T axis to be $\Theta = -61.76$ K. The negative Θ value suggests the predominance of antiferromagnetic exchange interactions in the sample. The value of the effective magnetic moment can be calculated to be $\mu_{eff} = 6.93\ \mu_B$, which is higher than the theoretical moment (5.92 μ_B) for Mn^{2+} by considering a spin only magnetism.

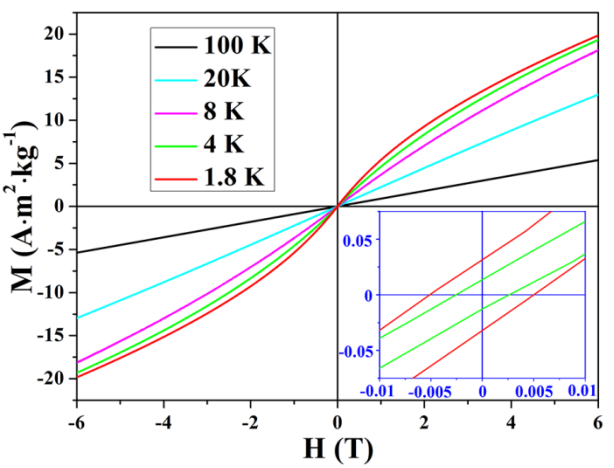

Fig. 5 Magnetization hysteresis loops measured at 1.8, 4, 8, 20 and 100 K in ZFC mode for the as-synthesized $MnNb_2O_6$ ellipsoidal sample. The inset presents the corresponding zoom view of the hysteresis loops of 1.8 and 4 K at low magnetic fields.

To further investigate the magnetic properties of the as-synthesized $MnNb_2O_6$ ellipsoidal structures, the magnetization as a function of applied magnetic field was measured at different temperatures (1.8, 4, 8, 95, 20, and 100 K) displayed in Fig. 5. Actually, in these five M–H curves, only the hysteresis loops at 1.8 and 4 K are open according to the corresponding zoom view at low magnetic fields as shown in the inset, which confirms the antiferromagnetic structure and the presence of a ferromagnetic moment. The coercivity is determined as about 4 and 2 $kA \cdot m^{-1}$ for the hysteresis loop at 1.8 and 4 K, respectively. No obvious saturation can be established up to H = 6 T, further suggesting the predominant antiferromagnetic ordering. As for the M–H curve at 8 K, it looks like a S-shaped line rather than a straight line, so the coercivity and remanence can be taken as zero. The absence of opening in hysteresis loop suggests the presence of superparamagnetic state. Accordingly, considering the finite size of the constituent nanoparticles, the possibility of superparamagnetic blocking may be expected in the sample. While the measurement temperature is enhanced to above 20 K, as expected from the ~~M~~ results, the magnetization linearly increases with the applied field, signifying the typical paramagnetic phase.

Microwave absorption properties

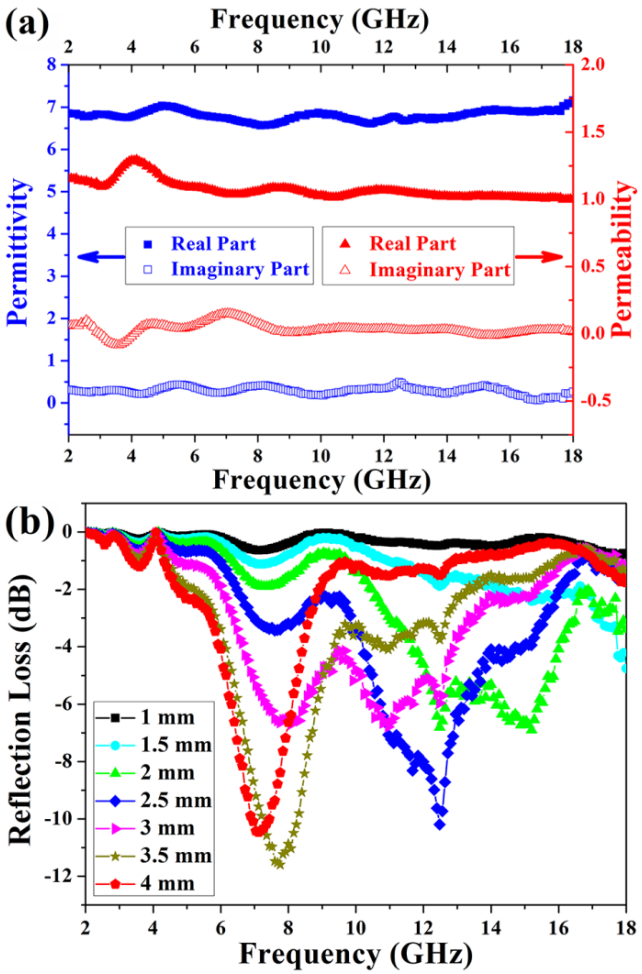

Fig. 6 The frequency dependence of (a) the complex permittivity and permeability, and (b) the reflection loss with various thicknesses of the as-prepared $MnNb_2O_6$ ellipsoidal sample.

Complex permittivity and permeability of materials are associated with their microwave absorption properties. As is well known, the real parts of complex permittivity and permeability represent the storage of electric and magnetic energy, while the imaginary parts of complex permittivity and permeability stand for the loss of electric and magnetic energy, respectively. Fig. 6a shows the real parts and imaginary parts of the relative complex permittivity and permeability of the as-obtained ellipsoidal $MnNb_2O_6$ hierarchical nanostructures as a function of frequency. It can be seen that all these four parameters are nearly constant with small fluctuation over the whole test range of 2–18 GHz. Mostly, however, the imaginary permittivity of the sample has a relatively small value of 0.25–0.5. In general, the higher imaginary part implies more dielectric loss and makes more electromagnetic energy transfer into heat energy. Hence, it can be deduced that the microwave absorption property of this sample is not very satisfactory. Interestingly, it is observed that the imaginary permeability of the sample is negative between 3 and 4 GHz, implying that the magnetic energy is radiated out from the sample probably owing to the motion of charges.[27-28]

Based on the transmission line theory, the electromagnetic reflection loss (RL) of the sample can be calculated from the permittivity and permeability at the given frequency and absorber thicknesses in terms of the following equations:

$$Z_{in} = Z_0(\mu_r/\varepsilon_r)^{1/2}\tanh[j(2\pi fd/c)(\mu_r\varepsilon_r)^{1/2}]$$

$$RL = 20\log|(Z_{in} - Z_0)/(Z_{in} + Z_0)|$$

where Z_0 is the impedance of free space, Z_{in} is the input impedance of absorber, μ_r and ε_r are the relative complex permeability and permittivity, respectively, f is the frequency of incident electromagnetic wave, d is the thickness of absorber, and c is the velocity of light. According to the equations above, the simulations of the RL for the as-prepared $MnNb_2O_6$ sample with different matching thicknesses are shown in Fig. 6b. The typical microwave absorption property can be clearly observed. It is found that both the RL intensity and the frequency of RL minimum depend on the thickness. First, with increasing the thickness, the minimum reflection loss obviously shifts from higher frequency region to lower one. Second, there is an optimal absorbing thickness for the minimum reflection loss. The absorption peak reaches the minimum value of −11.6 dB at 7.8 GHz when the thickness of absorber is 3.5 mm, and the absorption bandwidth lower than −10 dB is about 1.1 GHz (from 7.2 to 8.3 GHz). It should be noted that Pullar et al.[1,6] and Lee et al.[3-4] have demonstrated the resonant microwave frequencies of 6.77 and 10 GHz, respectively, for $MnNb_2O_6$ compounds. Therefore, although the prepared $MnNb_2O_6$ sample has a much lower permittivity, it still exhibits the reflection losses at similar frequencies (7~8 GHz). The as-obtained $MnNb_2O_6$ hierarchical ellipsoids exhibit two typical characteristics: first, the radially distributed nanoflakes would be beneficial for diffuse scattering of the incident microwaves, which results in a strong absorption of microwave; second, these upstanding nanoflakes consisting of nanoparticles have a very small thickness, a point discharge effect may be expected when a strong electromagnetic field is applied, which also contributes to strong absorption.

Conclusions

In summary, a facile hydrothermal process has been successfully

employed to fabricate $MnNb_2O_6$ ellipsoids with flake-like hierarchical structures, which consist of nanoparticles in diameters of about 10–20 nm. The magnetization versus temperature results reveal the antiferromagnetic order at $T_N \approx 4$ K. The isothermal magnetization data exhibit the opening-up of magnetic hysteresis loops below T_N (at 1.8 and 4 K), corresponding to the presence of a ferromagnetic moment. A small coercivity of 4 and 2 $kA \cdot m^{-1}$ is obtained at 1.8 and 4 K, respectively. It is interesting that the superparamagnetic state may be observed at 8 K due to the small size effect. The microwave absorption data show that the absorbing peak shifts to lower frequency region with increasing the absorber thickness. The value of the minimum reflection loss is − 11.6 dB at 7.8 GHz for the as-synthesized $MnNb_2O_6$ ellipsoidal hierarchical nanostructures with a matching thickness of 3.5 mm, and an absorption band under −10 dB from 7.2 to 8.3 GHz can be detected. In the long run, this synthetic approach should be expected to be extendable for the general synthesis of a series of columbite niobate ceramics and their solid solutions.

Acknowledgements

Financial supports by National Natural Science Foundation of China (21001062), the Research Fund for the Doctoral Program of Higher Education of China (20093601120010) and the Natural Science Foundation of Jiangxi Province (20132BAB216016) are gratefully acknowledged.

Notes and references

[a] *School of Materials Science and Engineering, Nanchang University, Nanchang, Jiangxi 330031, P. R. China. Fax: 86 791 83969329; E-mail: shjlei@ncu.edu.cn*

[b] *School of Chemistry and Chemical Engineering, Liaocheng University, Liaocheng, Shandong 252059, P. R. China.*

1 R. C. Pullar, *J. Am. Ceram. Soc.*, 2009, **92**, 563–577.
2 D. Prabhakaran, F. R. Wondre and A. T. Boothroyd, *J. Cryst. Growth*, 2003, **250**, 72–76.
3 H. J. Lee, I. T. Kim and K. S. Hong, *Jpn. J. Appl. Phys.*, 1997, **36**, L1318–1320.
4 H. J. Lee, K. S. Hong, S. J. Kim and I. T. Kim, *Mater. Res. Bull.*, 1997, **32**, 847–855.
5 R. C. Pullar, C. Vaughan and N. McN. Alford, *J. Phys. D: Appl. Phys.*, 2004, **37**, 348–352.
6 R. C. Pullar, J. D. Breeze and N. McN. Alford, *J. Am. Ceram. Soc.*, 2005, **88**, 2466–2471.
7 R. C. Pullar, J. D. Breeze and N. McN. Alford, *Key Eng. Mater.*, 2002, **224-226**, 1–4.
8 T. Kolodiazhnyi, A. Petric, A. Belous, O. V'yunov, and O. Yanchevskij, *J. Mater. Res.*, 2002, **17**, 3182–3189.
9 A. Belous, O. Ovchar, B. Jancar and J. Bezjak, *J. Eur. Ceram. Soc.*, 2007, **27**, 2933–2936.
10 L. M. Holmes, A. A. Ballman and R. R. Hecker, *Solid State Commun.*, 1972, **11**, 409–413.
11 O. V. Nielsen, B. Lebech, F. K. Larsen, L. M. Holmes and A. A. Ballman, *J. Phys. C: Solid State Phys.*, 1976, **9**, 2401–2411.
12 C. Tealdi, M. C. Mozzati, L. Malavasi, T. Ciabattoni, R. Amantea and C. B . Azzoni, *Phys. Chem. Chem. Phys.*, 2004, **6**, 4056–4061.
13 F. García-Alvarado, A. Orera, J. Canales-Vázquez and J. T. S. Irvine, *Chem. Mater.*, 2006, **18**, 3827–3834.
14 A. Orera, F. García-Alvarado and J. T. S. Irvine, *Chem. Mater.*, 2007, **19**, 2310–2315.
15 M. E. Arroyo y de Dompablo, Y. L. Lee and D. Morgan, *Chem. Mater.*, 2010, **22**, 906–913.
16 A. Martínez-de la Cruz, N. L. Alcaraz, A. F. Fuentes and L. M. Torres-Martínez, *J. Power Sources*, 1999, **81-82**, 255–258.
17 A. N. Mansurova, R. I. Gulyaeva, V. M. Chumarev and V. P. Mar'evich, *J. Therm. Anal. Calorim.*, 2010, **101**, 45–47.
18 H. Weitzel, *Z. Anorg. Allg. Chem.*, 1971, **380**, 119–127.
19 B. E. Davaadorj, H. Jeon and J. Lee, *J. Alloy. Compd.*, 2012, **527**, 122–126.
20 A. Bartels, F. Holtz and R. L. Linnen, *Am. Mineral.*, 2010, **95**, 537–544.
21 L. Z. Zhang, G. Garnweitner, I. Djerdj, M. Antonietti and M. Niederberger, *Chem. Asian J.*, 2008, **3**, 746–752.
22 W. B. Hu, Y. M. Zhao, Z. L. Liu, C. W. Dunnill, D. H. Gregory and Y. Q. Zhu, *Chem. Mater.*, 2008, **20**, 5657–5665.
23 W. B. Hu, Z. C. Cui, Y. Z. Mi, *Mater. Chem. Phys.*, 2012, **133**, 599–604.
24 B. M. Wanklyn, B. J. Garrard and G. Garton, *Mater. Res. Bull.*, 1976, **11**, 1497–1501.
25 A. A. Ballman, *J. Am. Ceramic Soc.*, 1965, **48**, 112–113.
26 C. M. Flynn, Jr., and G. D. Stucky, *Inorg. Chem.*, 1969, **8**, 178–180.
27 Q. L. Liu, D. Zhang and T. X. Fan, *Appl. Phys. Lett.*, 2008, **93**, 013110.
28 Y. B. Li, G. Chen, Q. H. Li, G. Z. Qiu and X. H. Liu, *J. Alloy. Compd.*, 2011, **509**, 4104–4107.

Graphical Abstract

Preparation, Magnetic and Microwave Absorption Properties of $MnNb_2O_6$ Ellipsoid-Like Hierarchical Structures

Shuijin Lei,*[a] Donghai Guo,[a] Chuanning Wang,[a] Di Cheng,[a] Xijie Gao,[a] Suyuan Zeng,[b] Yanhe Xiao,[a] and Baochang Cheng[a]

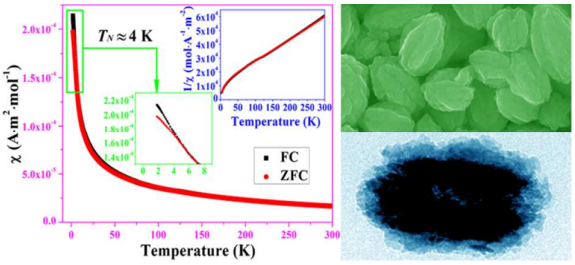

The $MnNb_2O_6$ ellipsoidal hierarchical structures exhibiting antiferromagnetic behavior with $T_N \approx 4$ K are fabricated by a facile hydrothermal method.